© 2020. Published by The Company of Biologists Ltd | Journal of Cell Science (2020) 133, jcs242214. doi:10.1242/jcs.242214

RESEARCH ARTICLE

Microtubule motor transport in the delivery of melanosomes to the actin-rich apical domain of the retinal pigment epithelium

Mei Jiang[1,2,*], Antonio E. Paniagua[1,2], Stefanie Volland[1,2], Hongxing Wang[1,2], Adarsh Balaji[1,2], David G. Li[1,2], Vanda S. Lopes[1,2], Barry L. Burgess[1,2] and David S. Williams[1,2,3,4,‡]

ABSTRACT

Melanosomes are motile, light-absorbing organelles that are present in pigment cells of the skin and eye. It has been proposed that melanosome localization, in both skin melanocytes and the retinal pigment epithelium (RPE), involves melanosome capture from microtubule motors by an unconventional myosin, which dynamically tethers the melanosomes to actin filaments. Recent studies with melanocytes have questioned this cooperative capture model. Here, we test the model in RPE cells by imaging melanosomes associated with labeled actin filaments and microtubules, and by investigating the roles of different motor proteins. We found that a deficiency in cytoplasmic dynein phenocopies the lack of myosin-7a, in that melanosomes undergo fewer of the slow myosin-7a-dependent movements and are absent from the RPE apical domain. These results indicate that microtubule-based motility is required for the delivery of melanosomes to the actin-rich apical domain and support a capture mechanism that involves both microtubule and actin motors.

KEY WORDS: Melanosome, Retina, Dynein, Kinesin-1, Myosin-7a

INTRODUCTION

Melanosomes are organelles that originate from endosomes and contain melanin pigments (Marks and Seabra, 2001). They are present in the skin and the eye. An important function of melanosomes is in the screening of light, which can be a dynamic process, effected by melanosome motility, in response to changes in ambient lighting. Because melanosomes can be imaged with standard bright-field microscopy, without overexpression of tagged protein markers, they represent an excellent system for investigating organelle motility and the molecular motor systems that drive the underlying transport.

In mammalian skin, melanosome biogenesis occurs in melanocytes (Raposo and Marks, 2007). The melanosomes then pass from the dendrites of the melanocytes to neighboring keratinocytes (Hume et al., 2001; Wasmeier et al., 2008; Fukuda, 2013; Wu and Hammer, 2014; Moreiras et al., 2019). Preceding the intercellular transfer, melanosomes must be transported and retained in the melanocyte dendrites. Retention of the melanosomes depends on myosin-5a. Early studies showed that the melanocyte dendrites in *Myo5a*-null mice (known as *dilute* mice because of their light coat color) do not contain melanosomes (Provance et al., 1996; Wei et al., 1997). It was then shown that myosin-5a is linked to melanosomes by RAB27A and a member of the exophilin family, melanophilin. Live-cell studies led to a model in which melanosomes are transported to the cell periphery by microtubule motors and then passed onto myosin-5a, which retains them in the dendrite (i.e. a cooperative capture model) (Wu et al., 1998; Desnos et al., 2007; Hammer and Sellers, 2011). The main microtubule motor driving the movement to the periphery is indicated to be the plus-end directed motor kinesin-1 (Hara et al., 2000; Vancoillie et al., 2000). More recently, this model has been challenged, based on the lack of requirement for microtubule integrity for delivery of melanosomes to the dendrites, and lack of enrichment of kinesin-1 on melanosomes. Instead, recent evidence supports processive myosin-5a transport entirely from the center of the melanocyte to its periphery (Evans et al., 2014; Robinson et al., 2017).

In the eyes of invertebrates and vertebrates, movements of melanosomes provide a means to alter visual sensitivity and resolution. Clear examples are found among mollusks (Daw and Pearlman, 1974), arthropods (Williams, 1982; Narendra et al., 2016) and fish and amphibians (Back et al., 1965; Burnside, 2001). In the retinal pigment epithelium (RPE) of vertebrate eyes, cylindrically shaped melanosomes enter the narrow apical processes that project among the photoreceptor outer segments (POSs), with their long axis parallel to the POSs and thus the direction of incoming light (Burnside et al., 1983; Burgoyne et al., 2015). In lower vertebrates, movement into the apical processes upon light exposure and withdrawal from them upon darkness are major events, affording significant changes in the light-guiding properties of the POSs. Although more muted, melanosomes have been observed to move into the RPE apical processes of mice in response to light onset (Futter et al., 2004). The effect of this movement is unclear, but it might be related to functions other than light absorption that have been identified for RPE melanosomes. For example, melanosomes have been shown to have a cytoprotective effect in RPE cells under nonphotic oxidative stress (Burke et al., 2011). Melanosomes might also contribute to the enormous phagocytic load incurred by RPE cells; for example, in the mouse central retina each RPE cell is associated with 200 POSs (Volland et al., 2015) and, each day, peaking at light onset, the distal 10% of each POS is ingested and then degraded (Young, 1967; LaVail, 1976). RPE melanosomes contain proteases (Azarian et al., 2006), including cathepsin D, a major enzyme in the degradation of POS proteins (Hayasaka et al., 1975), and have been observed to fuse with phagosomes (Schraermeyer et al., 1999).

Although lack of myosin-5a does not affect the localization of RPE melanosomes (Gibbs et al., 2004), another unconventional myosin,

[1]Departments of Ophthalmology and Neurobiology, David Geffen School of Medicine at UCLA, Los Angeles, CA 90095, USA. [2]Stein Eye Institute, David Geffen School of Medicine at UCLA, Los Angeles, CA 90095, USA. [3]Molecular Biology Institute, David Geffen School of Medicine at UCLA, Los Angeles, CA 90095, USA. [4]Brain Research Institute, David Geffen School of Medicine at UCLA, Los Angeles, CA 90095, USA.
*Present address: Department of Ophthalmology, Shanghai General Hospital, Shanghai Jiao Tong University, School of Medicine, Shanghai, China, 200080.

‡Author for correspondence (dswilliams@ucla.edu)

A.E.P., 0000-0002-2526-8412; H.W., 0000-0003-4063-5417; D.G.L., 0000-0001-6334-1441; V.S.L., 0000-0002-2904-0247; B.L.B., 0000-0001-9279-2751; D.S.W., 0000-0002-7758-3932

Handling Editor: David Stephens
Received 25 November 2019; Accepted 25 June 2020

Journal of Cell Science (2020) 133, jcs242214. doi:10.1242/jcs.242214

myosin-7a, does. In humans, mutations in the gene encoding myosin-7a underlie Usher syndrome type 1B, a deaf-blindness disorder (Weil et al., 1995). One of several retinal functions for myosin-7a (Williams and Lopes, 2011) involves the apical localization of RPE melanosomes, including their presence in the apical microvilli (Liu et al., 1998). As for melanocyte melanosomes, RPE melanosomes require RAB27A for their localization but, instead of melanophilin, they require another exophilin (myosin VIIA and Rab interacting protein; MYRIP), which links RAB27A and myosin-7a (El-Amraoui et al., 2002; Futter et al., 2004; Gibbs et al., 2004; Kuroda and Fukuda, 2005; Klomp et al., 2007). Therefore, apical localization of RPE melanosomes is comparable to the dendritic localization of melanocyte melanosomes, with a RAB27A–MYRIP–myosin-7a complex used by the RPE in a similar way as the RAB27A–MLPH–myosin-5a complex is used by melanocytes. However, the motility of melanosomes in the RPE cell body has not been specifically studied, and it is not known how melanosomes move from the RPE cell body to the apical region. Thus, a cooperative capture model has not been tested.

Melanosomes in primary cultures of RPE cells lacking myosin-7a undergo a larger number of fast long-range movements than in similarly cultured wild-type RPE cells (Gibbs et al., 2004; Lopes et al., 2007a). It was suggested that these faster movements are driven by microtubule motors. In the present study, we test this proposal by direct observation of the motility of RPE melanosomes in the presence of labeled actin filaments and microtubules. In addition, we identify microtubule motors that associate with the melanosomes and are required for the normal motility and localization of melanosomes. We compare and contrast our findings with reports on melanosome motility in melanocytes.

RESULTS

RPE melanosomes move along actin filaments

Previous studies have demonstrated that myosin-7a is required for normal melanosome localization (Liu et al., 1998) and motility dynamics (Gibbs et al., 2004; Lopes et al., 2007a) in RPE cells, suggesting that melanosomes are tethered to or move along actin filaments by this actin-based motor. We attempted to observe the interaction between melanosomes and actin filaments by direct imaging of live RPE cells isolated from wild-type mice and expressing RFP-actin or GFP-tractin; GFP-tractin labels only F-actin (Johnson and Schell, 2009; Yi et al., 2012). Imaging indicated that the melanosomes were associated with labeled actin filaments and were typically oriented with their long axis parallel to the filaments. Melanosomes were motionless for quite long periods, as if tethered to an actin filament, with occasional relatively short bursts of movement along the labeled actin filaments, with their long axis remaining in line with the direction of movement (Movies 1, 2). Fig. 1A shows the track of a melanosome along a labeled actin

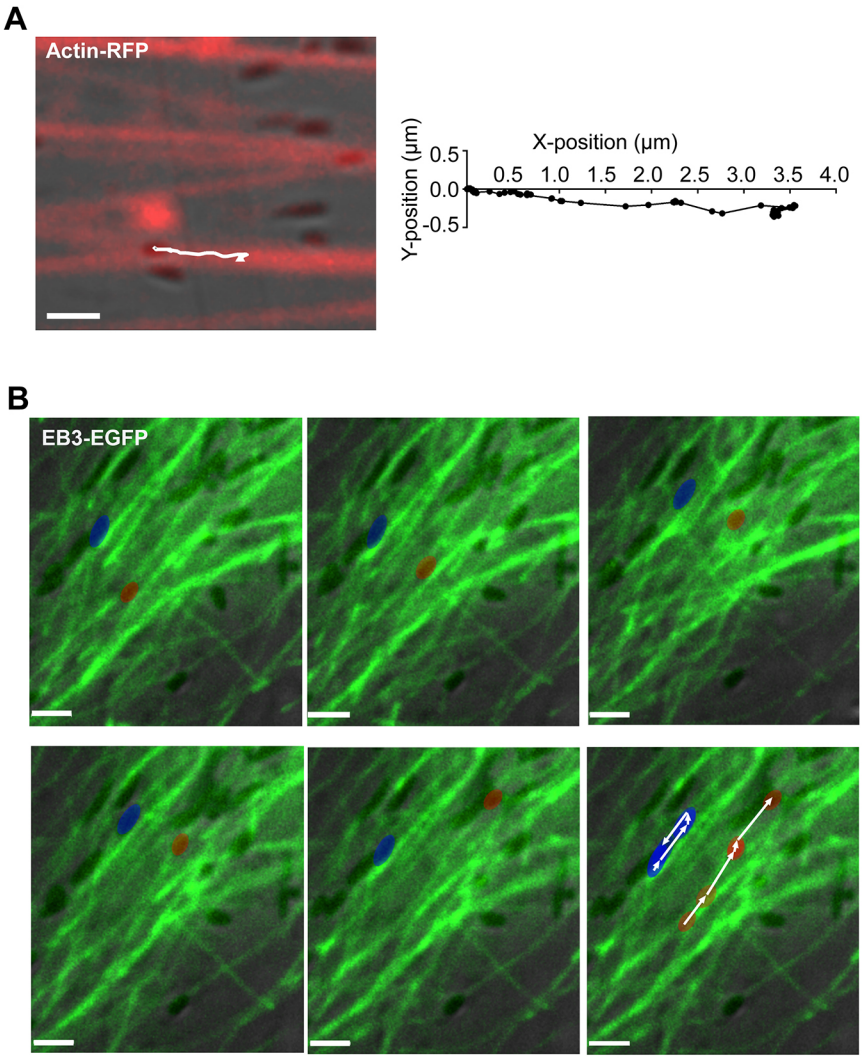

Fig. 1. Movement of melanosomes along actin filaments and microtubules in mouse primary RPE cells. (A) Movement of melanosomes along actin filaments in a cultured primary mouse RPE cell, transduced with Cellular Lights Actin-RFP. Single frame from the start of Movie 1. The white line shows the track that a melanosome takes along an actin filament, evident in subsequent frames. The track is shown in detail on the right. (B) Frames from Movie 3, showing movement of melanosomes along EB3-EGFP labeled microtubules in RPE cells isolated from shaker1 mice (in this case, the *shaker1*^{4626SB} allele, which is null for *Myo7a*). The blue pseudocolored melanosome moves first to the upper right, and then reverses course. The red pseudocolored melanosome undergoes a longer run towards the upper right. The complete tracks of the two melanosomes are shown in the last panel. The trajectories were obtained using Volocity software and are shown as a white line, with small arrowheads indicating the direction of movement. EB3-EGFP labels the microtubule growing (plus) ends, most of which (as shown in Movie 3) migrate to the lower left of the field of view. Scale bars: 2 μm.

Journal of Cell Science (2020) 133, jcs242214. doi:10.1242/jcs.242214

filament (or a bundle of parallel actin filaments), as demonstrated in Movie 1.

RPE melanosomes move along microtubules

As a first test of whether the fast long-range movements of RPE melanosomes occur along microtubules, we imaged melanosomes in primary cultures of shaker1 RPE cells that expressed tubulin-GFP or EB3-EGFP in order to label the microtubules fluorescently. We studied cells from *shaker1*^{4626SB} mice, which have a *Myo7a*-null mutation (Liu et al., 1999), in order to eliminate myosin-7a-based melanosome motility on actin filaments. Thus, we could isolate microtubule motility from myosin-7a-based motility on any (unlabeled) actin filaments that were close to the microtubules. Use of shaker1 RPE also increased the number of melanosomes available for microtubule movements (Gibbs et al., 2004; Lopes et al., 2007a).

Melanosomes were evident moving along the labeled microtubules (Fig. 1B; Movie 3). Compared with tracks along actin filaments in wild-type RPE cells (Fig. 1A; Movies 1, 2), this movement of melanosomes along microtubules occurred at faster speeds and with longer run lengths. Like the movement along actin filaments, the long axis of a melanosome remained aligned with the microtubule and thus the direction of movement. Movement in one direction was followed by at least one clear reversal of direction for 18% of the observed melanosomes during 3 min of imaging (see melanosome indicated by arrowhead in Fig. 1B). These bidirectional movements suggest the involvement of both plus-end and minus-end directed microtubule motors. Fast melanosome movements were also observed along labeled microtubules in wild-type RPE cells, although they occurred less frequently and over shorter distances.

Dependence on the presence of microtubules for melanosome motility has been shown previously; exposure of mouse primary RPE cells to 10 µm nocodazole for 1 h resulted in complete elimination of any motility in the majority of melanosomes (Lopes et al., 2007a). A similar finding was observed in the present study when comparing melanosome motility in untreated and nocodazole-treated mouse primary RPE cultures. The melanosomes that still moved in nocodazole-treated cells underwent only short-range movements at slow speeds (Fig. 2), of the type attributed to myosin-7a motility on actin filaments (Gibbs et al., 2004; Lopes et al., 2007a).

For the remainder of the study, we tested the roles of kinesin-1 and cytoplasmic dynein in driving this microtubule motility.

Kinesin-1 involvement in RPE melanosome transport

Studies on kinesin-1 indicate that it functions in RPE phagosome motility (Jiang et al., 2015), although not in the motility of melanosomes in melanocytes (Robinson et al., 2017). To investigate whether kinesin-1 plays a role in RPE melanosome motility, we focused on its ubiquitous heavy chain, KIF5B (Xia et al., 1998). In support of a role, immuno-electron microscopy (immunoEM) of retinal sections showed that KIF5B was associated with melanosomes. Immunogold label was detected on melanosomes in all regions of the cell (Fig. 3), although quantification of the label (from 80 fields of view, aggregated from sections from three animals) showed that melanosomes in the cell body contained 2.2 times more label than those in the apical microvilli, indicating a somewhat higher association between KIF5B and melanosomes in the region containing microtubules (Jiang et al., 2015).

To test for the involvement of KIF5B in melanosome transport, conditional knockout mice (Cui et al., 2011) were studied. Primary RPE cells isolated from *Kif5b*$^{flox/flox}$ mice were transfected with a Cre/GFP coexpression vector. Western blot analysis showed near complete depletion of KIF5B in the presence of Cre (Fig. 4A). Tracks of melanosome movements were obtained by imaging cells in primary RPE cultures from *Kif5b*$^{flox/flox}$ mouse littermates, with Cre expression (indicated by GFP) and without Cre expression. Analysis of the tracks showed that Cre expression resulted in a small shift in the distribution of measured maximal speeds, such that there was a lower frequency of slower maximal speeds ($\leq$0.6 µm s^{-1}) and a higher frequency of faster maximal speeds ($\geq$0.8 µm s^{-1}) (Fig. 4B).

These results suggest that KIF5B (and thus kinesin-1) contributes to the normal motility of melanosomes on microtubules. However, the change in motility was not associated with a significant change in the distribution of melanosomes in the RPE. The RPE in retinal sections from *Kif5b*$^{flox/flox}$;*BEST1-Cre* mice contained melanosomes in their apical microvilli as well as in the cell body, as in comparable sections from control mice (Fig. 4C).

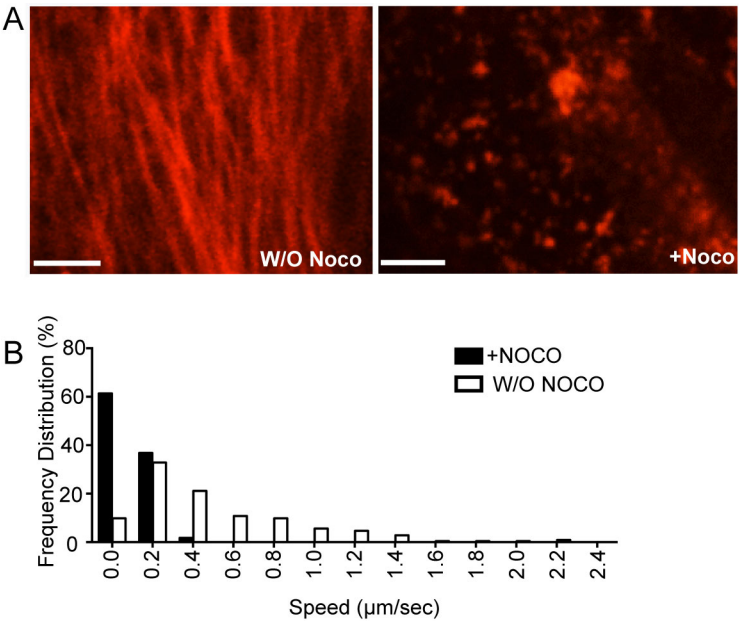

Fig. 2. Effect of nocodazole disruption of microtubules on melanosome motility in RPE cells. (A) Primary wild-type mouse RPE cells were transfected with tubulin-mCherry and treated with 10 µM nocodazole (Noco). Cells were imaged before (left) and 30 min after (right) treatment with nocodazole. (B) Distribution of speeds of melanosomes that were motile in nocodazole-treated and untreated cultures; note that more than 80% of melanosomes were immotile following nocodazole treatment (and thus not counted). Melanosomes were imaged at 2 frames/s and speeds determined from the frame-to-frame displacement (also known as instantaneous speed). Speeds were binned, such that speeds <0.2 µm s^{-1} were collected under 0 µm s^{-1}, speeds $\geq$0.2 but <0.4 µm s^{-1} were collected under 0.2 µm s^{-1}, etc. Scale bars: 5 µm.

Journal of Cell Science (2020) 133, jcs242214. doi:10.1242/jcs.242214

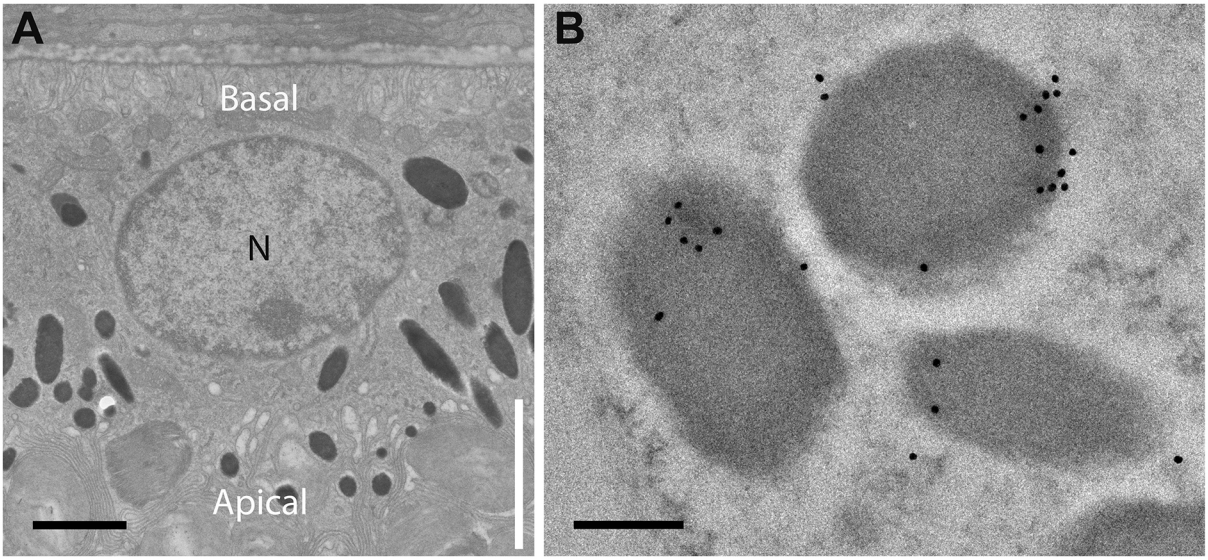

Fig. 3. Immunogold labeling of melanosomes in mouse RPE cells by KIF5B antibodies. (A) EM of mouse RPE cell. The apical region of the cell includes the apical microvilli (region indicated by vertical white line). These microvilli interdigitate with the tips of photoreceptor outer segments. The actual boundary between the actin-rich apical domain and the cell body (which contains microtubules throughout) corresponds to the level of the junctional complexes and a circumferential ring of actin filaments, and so is slightly more basal than the base of the microvilli (Jiang et al., 2015). N, nucleus. (B) Example of melanosomes labeled by KIF5B immunogold in the cell body region. Scale bars: 1 µm (A), 200 nm (B).

Dynein involvement in RPE melanosome transport

To test for evidence of melanosome transport by cytoplasmic dynein, we first performed immunoEM with antibodies against both intermediate chains of cytoplasmic dynein 1 (DYNC1). Similar to the result obtained with KIF5B immunoEM, melanosomes were labeled (Fig. 5A) and the density of melanosome label in the basal RPE was 2.4 times that measured on melanosomes in the apical microvilli (quantified from 47 fields of view, aggregated from sections from three animals).

Next, we used dynein heavy chain (DYNC1H1) shRNA, as described and characterized previously in a study of axonal transport in mouse neurons (Encalada et al., 2011), to investigate the effect of reducing the amount of DYNC1 heavy chain. We tested the efficacy of this shRNA in reducing DYNC1 intermediate chain expression using lentiviral transduction of primary RPE cultures, so that the majority of cells expressed the shRNA plasmids. Fig. 5B illustrates significant depletion of DYNC1 intermediate chains with the DYNC1H1 shRNA, in contrast to no effect with a scrambled shRNA.

Using subretinal injection and electroporation, we were able to transfect RPE cells with DYNC1H1 shRNA, and thus knock down RPE DYNC1 activity *in vivo*. In the areas of the retina transfected with DYNC1H1 shRNA, melanosomes were absent from the apical RPE; they did not surround the tips of the photoreceptor outer segments as in RPE that was not transfected or was transfected with

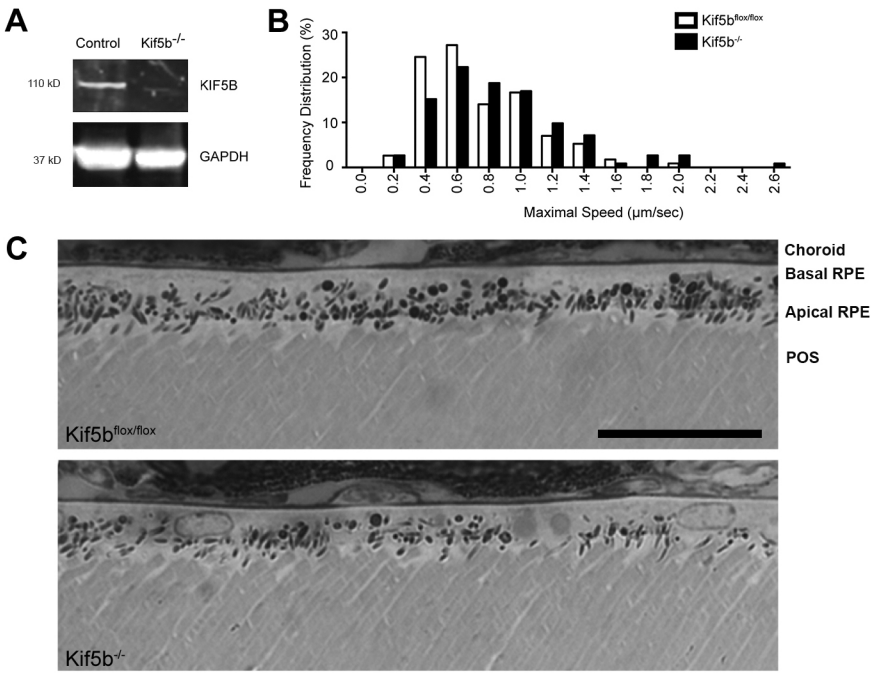

Fig. 4. Effect of loss of KIF5B on melanosome speed and localization. (A) Western blot of RPE cells isolated from *Kif5b*$^{flox/flox}$ mice transfected with Cre (to generate *Kif5b*$^{-/-}$) or without Cre (control). The blot was probed with antibodies against KIF5B and GAPDH (loading control). Apparent molecular masses are indicated. (B) Frequency distribution of the maximal speed measured over 3 min intervals for melanosomes in *Kif5b*$^{flox/flox}$ primary RPE cultures, with Cre (*Kif5b*$^{-/-}$) or without Cre (*Kif5b*$^{flox/flox}$). Data were obtained from 3 min tracks (n=56 tracks for *Kif5b*$^{-/-}$, n=57 tracks for *Kif5b*$^{flox/flox}$, aggregated from 3 separate experiments) of active melanosomes (i.e. with straight-line displacement of more than 2 µm after 3 min). Maximal speeds were binned, such that speeds <0.2 µm s^{-1} were collected under 0 µm s^{-1}, speeds ≥0.2 but <0.4 µm s^{-1} were collected under 0.2 µm s^{-1}, etc. (C) Light microscopy images of retinas from *Kif5b*$^{flox/flox}$ mice (*Kif5b*$^{flox/flox}$) and *Kif5b*$^{flox/flox}$*;BEST1-cre* (*Kif5b*$^{-/-}$) mouse retinas. The different retinal layers, choroid, basal RPE, apical RPE and the photoreceptor outer segments (POS), are indicated in the top panel. Scale bar: 25 µm.

Journal of Cell Science (2020) 133, jcs242214. doi:10.1242/jcs.242214

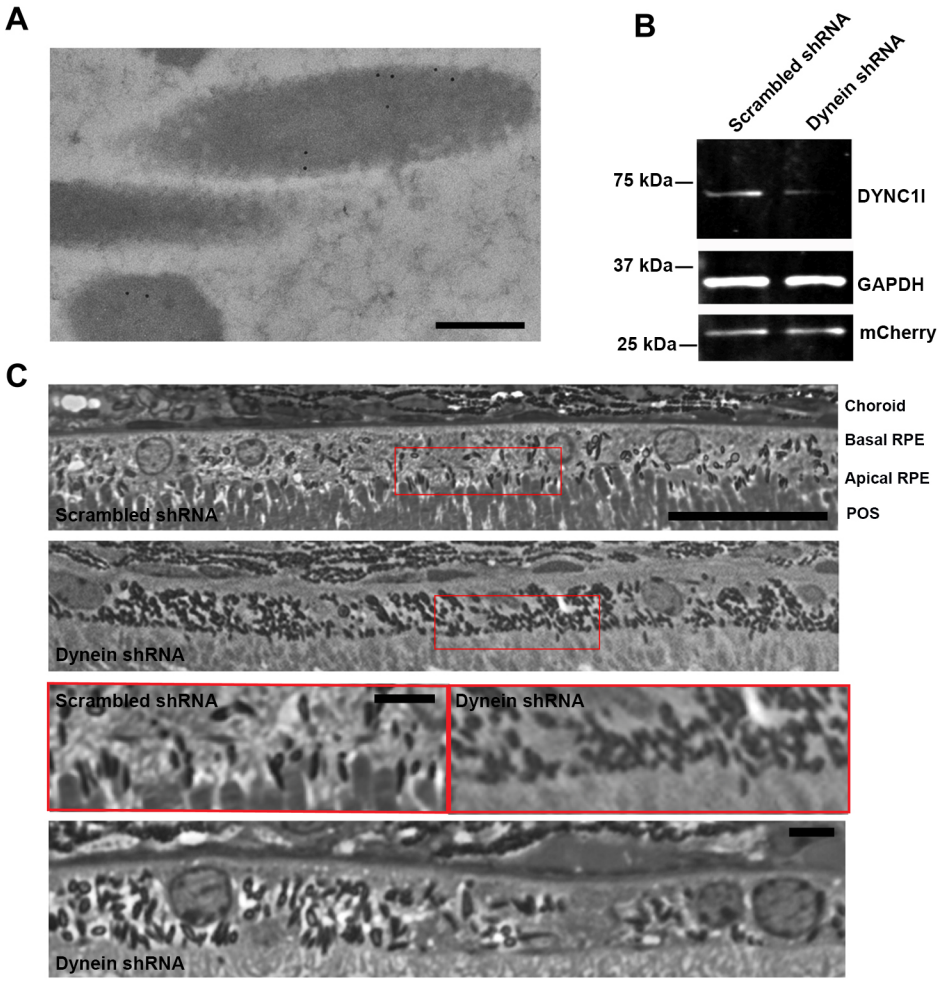

Fig. 5. Immunogold labeling of dynein and analysis of the effect of dynein deficiency on melanosome localization. (A) Example of melanosomes in the cell body region, labeled by antibodies against both intermediate chains of cytoplasmic dynein 1. (B) Western blot of RPE cell cultures transduced with lentivirus containing scrambled shRNA-mCherry or cytoplasmic dynein heavy chain (DYNC1H1) shRNA-mCherry. The blot was probed with antibodies against cytoplasmic dynein 1 intermediate chains 1 and 2 (DYNC1I), GAPDH (loading control) and mCherry (transduction control). (C) Light microscopy images of RPE cells from wild-type mice, injected subretinally with scrambled shRNA or DYNC1H1 shRNA. The different retinal layers, choroid, basal RPE, apical RPE and the photoreceptor outer segments (POS), are indicated in the top panel. The regions framed by the red boxes (top two panels) are shown at higher magnification in the next panel. The image in the bottom panel is from another retina that was injected with DYNC1H1 shRNA. In the scrambled shRNA-treated retinas, melanosomes were present in the apical RPE, whereas in the DYNC1H1 shRNA-treated retinas, melanosomes were largely absent from the apical RPE. The shRNA plasmids were delivered to the RPE cells by injection into the subretinal space, followed by electroporation. The regions of the retina examined corresponded to those near the site of plasmid injection, and therefore their relative location varied somewhat from animal to animal. Note that the number of melanosomes per RPE cell varies across normal mouse and rat retinas, even though melanosomes are still present in the apical processes of all regions (Howell et al., 1982; Williams et al., 1985). Scale bars: 200 nm (A), 25 µm (C, top two and bottom panels), 10 µm (C, third panel).

scrambled shRNA (Fig. 5C). Although the melanosomes were absent from the apical RPE, they did not congregate in a particular region of the cell body; they appeared to be distributed throughout the cell body, like melanosomes in wild-type RPE, and, indeed, like melanosomes in *Myo7a*-mutant mice (Liu et al., 1998).

To test how loss of DYNC1 affects melanosome motility, we tracked melanosomes in primary RPE cell cultures transfected with DYNC1H1 shRNA or scrambled shRNA (as a control). Treated cells in the culture could be identified by expression of mCherry. DYNC1H1 shRNA shifted the distribution of maximal melanosome speeds, such that there was a lower frequency of slow maximal speeds ($<0.4\ \mu m\ s^{-1}$) and a higher frequency of faster maximal speeds ($\geq 0.6\ \mu m\ s^{-1}$), compared with the effect of scrambled shRNA (Fig. 6A). The extent of this change in the distribution of maximal speeds was much more marked than that observed with the deletion of KIF5B; it was comparable to that observed in shaker1 mice as a result of loss of myosin-7a function (Gibbs et al., 2004; Lopes et al., 2007a).

We examined the effects of DYNC1 knockdown further by studying shaker1 RPE, so that melanosomes would not be recruited to actin filaments by myosin-7a, thus helping isolate motility on microtubules. As noted, loss of myosin-7a results in faster speeds of the motile melanosomes (Gibbs et al., 2004; Lopes et al., 2007a). This effect can be seen by comparing the control (scrambled shRNA) bars in Fig. 6A with those in Fig. 6C. In shaker1 RPE, DYNC1 knockdown resulted in reduction of the proportion of motile melanosomes from 30% to just 10% (Fig. 6B). Interestingly, DYNC1 knockdown did not significantly alter the distribution of maximal speeds of those melanosomes that were motile (Fig. 6C). It appears that the shift to a higher frequency of faster speeds with DYNC1 knockdown is a result of reduced delivery of melanosomes to the actin filaments and reduced myosin-7a motility, consistent with the observations of retinal sections (Fig. 5C).

Journal of Cell Science (2020) 133, jcs242214. doi:10.1242/jcs.242214

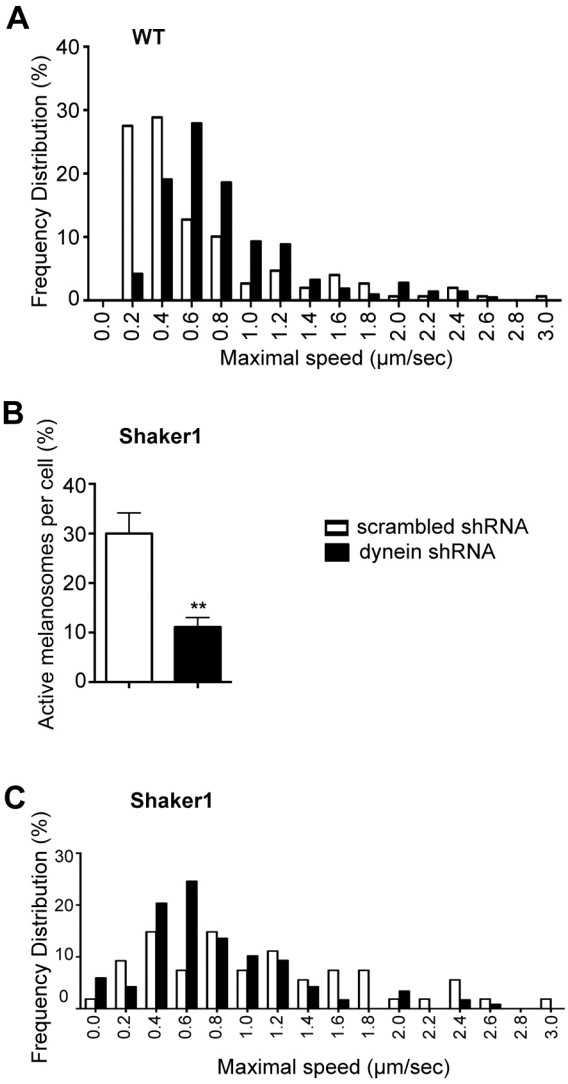

Fig. 6. Effect of loss of dynein on melanosome motility. (A–C) White bars, scrambled shRNA; black bars, DYNC1H1 shRNA. (A) Frequency distribution of the maximal speed measured for melanosomes in primary cultures of RPE cells treated with scrambled (control) shRNA or DYNC1H1 shRNA. Data were obtained from 3 min tracks (n=75 tracks for scrambled shRNA, n=106 tracks for DYNC1H1 shRNA, aggregated from three separate experiments) of active melanosomes (i.e. with straight-line displacement of more than 2 µm after 3 min). Maximal speeds were binned, such that speeds <0.2 µm s^{-1} were collected under 0 µm s^{-1}, speeds ≥0.2 but <0.4 µm s^{-1} were collected under 0.2 µm s^{-1}, etc. The percentage of active melanosomes, determined from three independent cell cultures, was similar for cells treated with scrambled shRNA (15±3% s.e.m.) and cells treated with DYNC1H1 shRNA (14±3% s.e.m.). (B) The percentage of active melanosomes (i.e. with straight-line displacement of more than 2 µm after 3 min) in shaker1 primary RPE cells, treated with scrambled shRNA or DYNC1H1 shRNA. Data were obtained from four separate experiments; **P=0.0007 (Mann–Whitney test, two-tailed). Error bars indicate s.e.m. (C) Frequency distribution of the maximal speed measured for melanosomes in primary cultures of shaker1 RPE cells treated with scrambled shRNA or DYNC1H1 shRNA. Data were obtained from 3 min tracks (n=27 tracks for scrambled control shRNA, n=60 tracks for dynein shRNA, aggregated from three separate experiments) of active melanosomes (i.e. with straight-line displacement of more than 2 µm after 3 min). Maximal speeds were binned as in A.

DISCUSSION

We report direct imaging of RPE melanosomes moving along labeled actin filaments and microtubules. The long axis of the melanosome is aligned with the actin filament or microtubule, and thus the direction of movement. Most melanosomes were paused on the actin filaments, as if tethered, and underwent relatively short movements. Movements along microtubules were faster, involved longer runs and were sometimes bidirectional. In addition, we investigated the roles of kinesin-1 and cytoplasmic dynein in driving melanosome motility along microtubules. ImmunoEM demonstrated that both motors were associated with melanosomes. Knockout of the kinesin-1 heavy chain gene, *Kif5b*, had a relatively mild effect, with no significant alteration in melanosome localization. However, shRNA knockdown of DYNC1H1 completely phenocopied lack of myosin-7a, in terms of melanosome motility in RPE cell culture and melanosome localization *in vivo*, indicating that cytoplasmic dynein is essential for the passage of melanosomes from the cell body to the actin-rich apical domain of the RPE.

The organization of microtubules in differentiated RPE cells is comparable to that of other epithelial cells (Bacallao et al., 1989; Gilbert et al., 1991), with some lateral microtubules emerging from an apical centrosome in the apical part of the cell body and some vertical microtubules, which are not associated with a centrosome. The majority (71%) of the vertical microtubules are oriented with their plus ends more basal (Jiang et al., 2015), so that minus-end directed movements direct melanosomes predominantly towards the RPE apical domain. A deficiency in dynein resulted in the same dislocalization of melanosomes from the apical RPE, and the same increase in motility, as observed with shaker1 RPE (Liu et al., 1998; Gibbs et al., 2004). Only a small minority of RPE cells contained any melanosomes in the actin-rich apical domain; perhaps DYNC1H1 was incompletely knocked down in these cells. In live RPE cells deficient in dynein, the distribution of maximal speeds was shifted away from the slower speeds that have been attributed to myosin-7a driven motility (Udovichenko et al., 2002). These findings indicate the importance of delivery of melanosomes to the minus-ends of the microtubules by dynein, so that they can be transferred from the cell body to the RAB27A–MYRIP–myosin-7a complex in the actin-rich apical domain. Thus, they support a cooperative capture model.

Despite evidence of some bidirectional movement of melanosomes on microtubules, and an effect on melanosome motility in response to loss of KIF5B, kinesin-1 had no obvious effect on melanosome localization. Loss of KIF5B resulted in a slight shift to faster maximal speeds (Fig. 4B). As with loss of DYNC1H1, this shift suggests fewer movements on actin filaments. However, the extent of the shift was much less than that observed with knockdown of dynein. Perhaps this milder phenotype is due to the involvement of another plus-end microtubule motor that normally functions with kinesin-1 in melanosome motility. The shift to faster maximal speeds in the absence of KIF5B suggests that such an additional motor mediates more rapid movements, which are inhibited in the presence of kinesin-1. Kinesin-1 and kinesin-3 have both been found to contribute to plus-end motility of cargoes in neuronal axons and HeLa cells (Guardia et al., 2016; Lim et al., 2017). Similarly, kinesin-1 and heterotrimeric kinesin-2 are both involved in the axonal transport of acetylcholine esterase vesicles (Kulkarni et al., 2017). Heterotrimeric kinesin-2 appears to be a good candidate to partner in melanosome motility, given its role in melanosome transport in *Xenopus* melanophores (Tuma et al., 1998).

An alternative possibility is that the absence of kinesin-1 results in more dynein motility. However, the *in vivo* speed of cytoplasmic dynein has been indicated to be slower than that of kinesin-1 (Howard, 2001), in which case, the observed shift to faster speeds seems inconsistent with increased dynein activity. Moreover, more dynein activity might be expected to be associated with a greater apical localization of melanosomes, which we did not detect.

Journal of Cell Science (2020) 133, jcs242214. doi:10.1242/jcs.242214

Skin melanocytes and RPE cells are two mammalian cell types in which melanosomes move from the cell body to the cell periphery. In melanocytes, melanosome biogenesis is active (Raposo and Marks, 2007) and the melanosomes do not return to the cell body; they are delivered to keratinocytes from the melanocyte dendrites (Hume et al., 2001; Wasmeier et al., 2008; Fukuda, 2013; Wu and Hammer, 2014; Moreiras et al., 2019). By contrast, melanosome biogenesis is very low in the postnatal RPE (Lopes et al., 2007b). Another difference between the two cell types is in the cytoskeletal organization. With the epithelial polarity and microtubule organization of RPEs (Jiang et al., 2015), movement towards the minus-ends of most microtubules directs melanosomes towards the actin-rich apical domain, where they can be captured by myosin-7a. In melanocytes, dynein moves melanosomes towards the cell nucleus, away from the dendrites (Byers et al., 2000), so that a plus-end microtubule motor is needed for movement towards the dendrites. It has been proposed that kinesin-1 fulfills this role, and is recruited to melanosomes by RAB1A (Ishida et al., 2012, 2015). However, more recently, it has been argued that KIF5B and RAB1A are not recruited to melanocyte melanosomes to a sufficient extent, and that the main driving force for the dendritic delivery of melanosomes comes from myosin-5a moving along cortical actin filaments (Evans et al., 2014; Robinson et al., 2017). In this case, melanocytes and RPE cells would differ, with a cooperative capture mechanism for melanosome delivery only present in RPE cells. However, consistent with the observations made here on kinesin-1 in RPEs, perhaps kinesin-1, together with another kinesin, functions in melanosome transport to the melanocyte dendrites and thus provides additional microtubule-based driving force.

MATERIALS AND METHODS

Animals

All procedures conformed to institutional animal care and use authorizations. The genetic mutants used were *Kif5b*$^{flox/flox}$ (JAX stock #008637) (Cui et al., 2011), *BEST1-cre* (Iacovelli et al., 2011) and shaker1 (*Myo7a*$^{4626SB/4626SB}$), which carries a premature stop codon, Q720X, and is an effective null (Liu et al., 1999). All mice had been backcrossed onto the C57BL/6HNsd (Harlan C57BL/6) genetic background and lacked the *Crb1*$^{rd8/rd8}$ mutation, as determined by PCR. *BEST1-cre* mice always contained only one transgenic allele. Breeding strategies and genotyping of the individual mutations followed those described previously (Holme and Steel, 2002; Cui et al., 2011; Iacovelli et al., 2011). Both genders of mice were used indiscriminately.

BEST1-cre transgenic mice were first crossed with *Kif5b*$^{flox/flox}$ *mice* to generate *Kif5b*$^{+/flox}$*;BEST1-cre* mice. Then *Kif5b*$^{+/flox}$*;BEST1-cre* mice were bred with *Kif5b*$^{flox/flox}$ mice to generate litters that included mice lacking functional *Kif5b* in the RPE (*Kif5a*$^{flox/flox}$*;BEST1-cre*). Genotyping was performed as described (Xia et al., 2003) to distinguished *Kif5a*$^{flox/flox}$*; BEST1-cre* mice from littermates.

All the mice were kept on a 12 h light/12 h dark cycle, under 10–50 lux fluorescent light during the light cycle.

Cell culture

RPE primary cells were isolated from mouse retinas as described previously (Gibbs et al., 2003; Gibbs and Williams, 2003). In brief, intact eyes were removed from 9- to 15-day-old mice and washed twice in DMEM (high glucose). They were then incubated with 2% (w/v) dispase in DMEM (high glucose) for 45 min at 37°C. The eyes were washed twice in growth medium (GM) that consisted of DMEM (high glucose), 10% FBS, 1% penicillin/streptomycin, 2.5 mM L-glutamax and 1× MEM nonessential amino acids. All reagents were from ThermoFisher Scientific. After removal of the anterior cornea, lens, capsule and iris-pigmented epithelium, the resulting posterior eyecups were incubated in GM for 20 min at 37°C. The neural retina was removed and sheets of RPE were then peeled off from Bruch's membrane, washed and cultured in complete GM at 37°C with an atmosphere of 5% CO_2.

For transfection prior to western blot analysis, primary RPE cells were plated for 24 h and then electroporated in suspension, using the Invitrogen Neon Transfection System 10µl kit (ThermoFisher Scientific), and then replated. For transfection of primary RPE cells, cultures were treated with Lipofectamine LTX (ThermoFisher Scientific), 1-2 days after plating. Transduction with lentiviral particles was done when the primary RPE cells were still in suspension. Analysis was performed 3-4 days post transfection or transduction in all cases.

Constructs and reagents

A short hairpin RNA (shRNA-mCherry) construct (modified pLentiLox3.7GW), targeted to cytoplasmic dynein heavy chain (DYNC1H1) (Encalada et al., 2011), and its scrambled negative control (D11, shRNA-mCherry) were provided by Sandra Encalada and Larry Goldstein (University of California, San Diego, La Jolla, CA). Packaging plasmids were pMD2.G and psPAX2 (Didier Trono, Addgene plasmids #12259 and #12260). LV-CIG vector (containing GFP downstream of Cre to achieve bicistronic expression) was used without lentiviral packaging vectors (Pfeifer et al., 2001). pEGFPN-EB3 was provided by Emilie Colin and Franck Perez (Institute Curie, Paris, France). F-tractin-GFP was provided by Michael Schell, Uniformed Services University (Johnson and Schell, 2009; Yi et al., 2012). All constructs were sequenced to confirm identity before use. CellLight Actin-RFP and CellLight Tubulin-RFP, packaged in baculovirus, were bought from ThermoFisher Scientific.

Western blot analysis

After transfection, cells were collected and lysed in 20 mM Tris-HCl pH 7.4, 5 mM $MgCl_2$, 10 mM NaCl, 1 mM DTT and 1× protease inhibitors (Sigma Aldrich). Equivalent amounts of sample were run on 4-12% NuPAGE Bis-Tris gel (ThermoFisher Scientific). After transfer, membranes were blocked with Odyssey blocking buffer (LI-COR; Lincoln) and probed with rabbit anti-KIF5B (Abcam ab5629) or mouse anti-DYNC1I (cytoplasmic dynein 1 intermediate chains 1 and 2; MAB1618, EMD Millipore), rabbit anti-RFP (PM005, MBL international) and mouse anti-GAPDH (MAB374, EMD Millipore). IRDye 800CW donkey anti-rabbit IgG, IRDye 680RD goat anti-mouse IgG, IRDye 680RD donkey anti-rabbit IgG or (LI-COR) were used as secondary antibodies. Membranes were imaged with the Odyssey infrared imaging system (LI-COR; Lincoln).

Live imaging and tracking analysis of melanosome motility

Sheets of mouse RPE cells were cultured in eight-well coverglass chambers (Labtek; ThermoFisher Scientific). Following dissection, cells were cultured for 1-2 days and then transfected or transduced. Cells were imaged 3-4 days after transfection or transduction using a spinning disk confocal microscope system (UltraVIEW ERS; PerkinElmer) containing a microscope (Axio Observer.A1; Carl Zeiss) fitted with an environment chamber. Melanosomes in cells in the center of the cultured patch were densely packed, and, although quite motile, were difficult to track. Tracking data were therefore obtained from cells away from the central region, where the melanosomes were more loosely packed but the cells were still at least partially polarized. Some time-lapse images were acquired with a 100× NA1.46 objective and a C9100-50 Hamamatsu Photonics camera. Other images were obtained with a 63× NA1.4 objective or a 100×, NA1.4, objective and a C11440-22CU Hamamatsu Photonics camera. All images of melanosomes were acquired and analyzed using Volocity software.

For the imaging of melanosomes moving along actin filaments or microtubules, cultured primary mouse RPE cells were transfected with F-tractin-GFP (Johnson and Schell, 2009) or pEGFPN-EB3 using Lipofectamine LTX (ThermoFisher Scientific), or transduced with CellLight actin-RFP (ThermoFisher Scientific). Single z-plane images were collected by a spinning disk confocal microscope.

To test for the effect of nocodazole, RPE cells were transduced with CellLight Tubulin-RFP (ThermoFisher Scientific). Cells were treated with 10 µM nocodazole for 30 min at 37°C and then imaged during a subsequent 30 min, in the same medium, at 2 frames/second by spinning disk confocal microscopy.

Motility analysis was performed on melanosomes that were tracked for 3 min and had a net displacement of at least 2 µm. A 'track' refers to the

trajectory of a melanosome during a 3 min interval and is represented by its X and Y coordinate series. 'Maximal speed' refers to the fastest instantaneous speed (frame to frame) during a 3 min track.

Statistical analyses were performed on Prism 6 (GraphPad). Mann–Whitney's test (two-tailed) was used for statistical analysis of melanosome tracks.

Subretinal injection and electroporation

Subretinal injection of 0.5 µl dynein (DYNC1H1) (3 µg µl^{-1}) shRNA or scrambled (D11) (3 µg µl^{-1}) shRNA plasmid was performed on postnatal day 2-4 mouse pups (Fig. S1), which were anesthetized by chilling on ice. The electroporation was conducted with 5 pulses at 80 V for 50 ms per pulse with 950 ms intervals. Pups were returned to their mother for at least 2 weeks.

Fluorescence microscopy for whole mount and cryosections

Whole mount and cryosections were performed as described previously (Jiang et al., 2015). Briefly, injected eyes were fixed in 4% formaldehyde overnight at 4°C, with a small cut on the cornea. The anterior segment was then removed. For RPE flat mounts, the eyecups were divided into quadrants, flattened and mounted for imaging. For cryosections, the posterior half of each eye was cryoprotected by processing through 15, 20 and 30% sucrose solutions in PBS and then embedded in OCT compound (Sakura). The cryosections were incubated with anti-RHO polyclonal antibody (pAb01) (Boesze-Battaglia et al., 1997; Liu et al., 1999) at 4°C overnight, followed by AlexaFluor 488-conjugated secondary antibody.

Light and immunoelectron microscopy

Eyes were enucleated from mice aged 1-2 months. The posterior eyecups were fixed by immersion in EM-grade 2% glutaraldehyde plus 2% formaldehyde (Electron Microscopy Sciences) in 0.1 M cacodylate buffer, then postfixed in 1% OsO_4 and processed for embedment in epon-812. For light microscopy, dorsoventral semithin (0.7 mm) sections were stained with toluidine blue and imaged under a microscope (Axiophot; Carl Zeiss) with a 63× NA1.4 oil objective (Carl Zeiss) and a camera (CoolSnap-Pro; Photometrics). Images were collected with Image-Pro Express software (Media Cybernetics). To investigate the localization of melanosomes within RPE cells, sets of eyes for each condition were obtained on least two separate occasions; from within each set, retinas were examined from a minimum of three animals for each condition.

For immunoEM, eyes were enucleated and fixed in 0.25% glutaraldehyde and 4% paraformaldehyde in 0.1 M cacodylate buffer at pH 7.4. Eyecups were dissected, washed in buffer and dehydrated in increasing concentrations of ethanol. After dehydration, tissue samples were infiltrated with LR White resin and polymerized at 55°C for 12-16 h. Ultrathin sections (70 nm) from the block were collected on formvar-coated nickel mesh grids, quenched for 15 min in 0.1 M glycine, washed in 0.1 M phosphate buffer and then blocked in 2% BSA for 20 min. Grids were washed again and incubated with anti-Kif5B (Abcam ab5629) or mouse anti-DYNC1I (cytoplasmic dynein 1 intermediate chains 1 and 2; MAB1618, EMD Millipore) in 1% native goat serum (NGS) overnight at 4°C. Grids were then washed and incubated with gold secondary antibodies (Jackson ImmunoResearch Laboratories, Baltimore, MD), diluted in 1% BSA for 90 min and washed three times with 0.1 M phosphate buffer. Contrast staining was performed with 5% uranyl acetate in 50% ethanol for 5 min, followed by triplicate washes with water. Images were taken on a transmission electron microscope (JEM-1200EX) at magnifications ranging from 30,000× to 80,000×. The primary antibodies were tested at dilutions of 1:200, 1:100 and 1:50; 18 nm anti-rabbit IgG or 12 nm anti-mouse IgG gold secondary antibodies were also tested at 1:20. For quantification, the primary antibodies were diluted 1:100 and the 18 nm anti-rabbit IgG was used as the secondary antibody. The number of gold particles per square micrometer of melanosome was determined to evaluate the association of kinesin and dynein with melanosomes in the RPE. Data were aggregated from sections obtained from six eyes. Background labeling levels were measured from the adjacent extracellular space and the photoreceptor outer segments, and the average was subtracted from the melanosome labeling results.

Acknowledgements

We thank Michael Schell (Uniformed Services University) for generously providing F-tractin plasmids, and Emilie Colin and Franck Perez (Institute Curie, Paris, France) for providing pEGFPN-EB3. We acknowledge the use of core equipment that was supported by the National Institutes of Health (P30EY0331) and a departmental Research to Prevent Blindness grant.

Competing interests

The authors declare no competing or financial interests.

Author contributions

Conceptualization: M.J., A.E.P., D.S.W.; Methodology: M.J., A.E.P., S.V., B.L.B., D.S.W.; Validation: M.J., A.E.P., S.V., H.W., A.B., D.G.L.; Formal analysis: M.J., A.E.P., H.W., A.B., D.G.L., D.S.W.; Investigation: M.J., A.E.P., S.V., H.W., A.B., D.G.L., B.L.B., V.S.L.; Resources: M.J., A.E.P., D.S.W.; Data curation: M.J., A.E.P., V.S.L.; Writing - original draft: M.J., D.S.W.; Writing - review & editing: M.J., A.E.P., D.S.W.; Visualization: M.J., A.E.P., S.V., A.B., D.G.L., B.L.B., V.S.L., D.S.W.; Supervision: S.V., B.L.B., V.S.L., D.S.W.; Project administration: D.S.W.; Funding acquisition: D.S.W.

Funding

The study was supported by a grant from the National Institutes of Health, R01EY027442 (to D.S.W.). Deposited in PMC for release after 12 months.

Supplementary information

Supplementary information available online at
https://jcs.biologists.org/lookup/doi/10.1242/jcs.242214.supplemental

Peer review history

The peer review history is available online at
https://jcs.biologists.org/lookup/doi/10.1242/jcs.242214.reviewer-comments.pdf

References

Azarian, S. M., McLeod, I., Lillo, C., Gibbs, D., Yates, J. R. and Williams, D. S. (2006). Proteomic analysis of mature melanosomes from the retinal pigmented epithelium. *J. Proteome Res.* **5**, 521-529. doi:10.1021/pr0502323

Bacallao, R., Antony, C., Dotti, C., Karsenti, E., Stelzer, E. H. and Simons, K. (1989). The subcellular organization of Madin-Darby canine kidney cells during the formation of a polarized epithelium. *J. Cell Biol.* **109**, 2817-2832. doi:10.1083/jcb.109.6.2817

Back, I., Donner, K. O. and Reuter, T. (1965). The screening effect of the pigment epithelium on the retinal rods in the frog. *Vision Res.* **5**, 101-111. doi:10.1016/0042-6989(65)90058-1

Boesze-Battaglia, K., Kong, F., Lamba, O. P., Stefano, F. P. and Williams, D. S. (1997). Purification and light-dependent phosphorylation of a candidate fusion protein, the photoreceptor cell peripherin/rds. *Biochemistry* **36**, 6835-6846. doi:10.1021/bi9627370

Burgoyne, T., O'Connor, M. N., Seabra, M. C., Cutler, D. F. and Futter, C. E. (2015). Regulation of melanosome number, shape and movement in the zebrafish retinal pigment epithelium by OA1 and PMEL. *J. Cell Sci.* **128**, 1400-1407. doi:10.1242/jcs.164400

Burke, J. M., Kaczara, P., Skumatz, C. M., Zareba, M., Raciti, M. W. and Sarna, T. (2011). Dynamic analyses reveal cytoprotection by RPE melanosomes against non-photic stress. *Mol. Vis.* **17**, 2864-2877.

Burnside, B. (2001). Light and circadian regulation of retinomotor movement. *Prog. Brain Res.* **131**, 477-485. doi:10.1016/S0079-6123(01)31038-5

Burnside, B., Adler, R. and O'Connor, P. (1983). Retinomotor pigment migration in the teleost retinal pigment epithelium. I. Roles for actin and microtubules in pigment granule transport and cone movement. *Invest. Ophthalmol. Vis. Sci.* **24**, 1-15.

Byers, H. R., Yaar, M., Eller, M. S., Jalbert, N. L. and Gilchrest, B. A. (2000). Role of cytoplasmic dynein in melanosome transport in human melanocytes. *J. Invest. Dermatol.* **114**, 990-997. doi:10.1046/j.1523-1747.2000.00957.x

Cui, J., Wang, Z., Cheng, Q., Lin, R., Zhang, X.-M., Leung, P. S., Copeland, N. G., Jenkins, N. A., Yao, K.-M. and Huang, J.-D. (2011). Targeted inactivation of kinesin-1 in pancreatic beta-cells in vivo leads to insulin secretory deficiency. *Diabetes* **60**, 320-330. doi:10.2337/db09-1078

Daw, N. W. and Pearlman, A. L. (1974). Pigment migration and adaptation in the eye of the squid, Loligo pealei. *J. Gen. Physiol.* **63**, 22-36. doi:10.1085/jgp.63.1.22

Desnos, C., Huet, S. and Darchen, F. (2007). 'Should I stay or should I go?': myosin V function in organelle trafficking. *Biol. Cell* **99**, 411-423. doi:10.1042/BC20070021

El-Amraoui, A., Schonn, J. S., Küssel-Andermann, P., Blanchard, S., Desnos, C., Henry, J. P., Wolfrum, U., Darchen, F. and Petit, C. (2002). MyRIP, a novel Rab effector, enables myosin VIIa recruitment to retinal melanosomes. *EMBO Rep.* **3**, 463-470. doi:10.1093/embo-reports/kvf090

Encalada, S. E., Szpankowski, L., Xia, C.-H. and Goldstein, L. S. (2011). Stable kinesin and dynein assemblies drive the axonal transport of mammalian prion protein vesicles. *Cell* **144**, 551-565. doi:10.1016/j.cell.2011.01.021

Evans, R. D., Robinson, C., Briggs, D. A., Tooth, D. J., Ramalho, J. S., Cantero, M., Montoliu, L., Patel, S., Sviderskaya, E. V. and Hume, A. N. (2014). Myosin-Va and dynamic actin oppose microtubules to drive long-range organelle transport. *Curr. Biol.* **24**, 1743-1750. doi:10.1016/j.cub.2014.06.019

Fukuda, M. (2013). Rab27 effectors, pleiotropic regulators in secretory pathways. *Traffic* **14**, 949-963. doi:10.1111/tra.12083

Futter, C. E., Ramalho, J. S., Jaissle, G. B., Seeliger, M. W. and Seabra, M. C. (2004). The role of Rab27a in the regulation of melanosome distribution within retinal pigment epithelial cells. *Mol. Biol. Cell* **15**, 2264-2275. doi:10.1091/mbc.e03-10-0772

Gibbs, D. and Williams, D. S. (2003). Isolation and culture of primary mouse retinal pigmented epithlelial cells. *Adv. Exp. Med. Biol.* **533**, 347-352. doi:10.1007/978-1-4615-0067-4_44

Gibbs, D., Kitamoto, J. and Williams, D. S. (2003). Abnormal phagocytosis by retinal pigmented epithelium that lacks myosin VIIa, the Usher syndrome 1B protein. *Proc. Natl. Acad. Sci. USA* **100**, 6481-6486. doi:10.1073/pnas.1130432100

Gibbs, D., Azarian, S. M., Lillo, C., Kitamoto, J., Klomp, A. E., Steel, K. P., Libby, R. T. and Williams, D. S. (2004). Role of myosin VIIa and Rab27a in the motility and localization of RPE melanosomes. *J. Cell Sci.* **117**, 6473-6483. doi:10.1242/jcs.01580

Gilbert, T., Le Bivic, A., Quaroni, A. and Rodriguez-Boulan, E. (1991). Microtubular organization and its involvement in the biogenetic pathways of plasma membrane proteins in Caco-2 intestinal epithelial cells. *J. Cell Biol.* **113**, 275-288. doi:10.1083/jcb.113.2.275

Guardia, C. M., Farías, G. G., Jia, R., Pu, J. and Bonifacino, J. S. (2016). BORC Functions upstream of kinesins 1 and 3 to coordinate regional movement of lysosomes along different microtubule tracks. *Cell Rep* **17**, 1950-1961. doi:10.1016/j.celrep.2016.10.062

Hammer, J. A., III and Sellers, J. R. (2011). Walking to work: roles for class V myosins as cargo transporters. *Nat. Rev. Mol. Cell Biol.* **13**, 13-26. doi:10.1038/nrm3248

Hara, M., Yaar, M., Byers, H. R., Goukassian, D., Fine, R. E., Gonsalves, J. and Gilchrest, B. A. (2000). Kinesin participates in melanosomal movement along melanocyte dendrites. *J. Invest. Dermatol.* **114**, 438-443. doi:10.1046/j.1523-1747.2000.00894.x

Hayasaka, S., Hara, S. and Mizuno, K. (1975). Degradation of rod outer segment proteins by cathepsin D. *J. Biochem. (Tokyo)* **78**, 1365-1367. doi:10.1093/oxfordjournals.jbchem.a131034

Holme, R. H. and Steel, K. P. (2002). Stereocilia defects in waltzer (Cdh23), shaker1 (Myo7a) and double waltzer/shaker1 mutant mice. *Hear. Res.* **169**, 13-23. doi:10.1016/S0378-5955(02)00334-9

Howard, J. (2001). *Mechanics of Motor Proteins and the Cytoskeleton*: Sinauer Associates Inc.

Howell, W. L., Rapp, L. M. and Williams, T. P. (1982). Distribution of melanosomes across the retinal pigment epithelium of a hooded rat: implications for light damage. *Invest. Ophthalmol. Vis. Sci.* **22**, 139-144.

Hume, A. N., Collinson, L. M., Rapak, A., Gomes, A. Q., Hopkins, C. R. and Seabra, M. C. (2001). Rab27a regulates the peripheral distribution of melanosomes in melanocytes. *J. Cell Biol.* **152**, 795-808. doi:10.1083/jcb.152.4.795

Iacovelli, J., Zhao, C., Wolkow, N., Veldman, P., Gollomp, K., Ojha, P., Lukinova, N., King, A., Feiner, L., Esumi, N. et al. (2011). Generation of Cre transgenic mice with postnatal RPE-specific ocular expression. *Invest. Ophthalmol. Vis. Sci.* **52**, 1378-1383. doi:10.1167/iovs.10-6347

Ishida, M., Ohbayashi, N., Maruta, Y., Ebata, Y. and Fukuda, M. (2012). Functional involvement of Rab1A in microtubule-dependent anterograde melanosome transport in melanocytes. *J. Cell Sci.* **125**, 5177-5187. doi:10.1242/jcs.109314

Ishida, M., Ohbayashi, N. and Fukuda, M. (2015). Rab1A regulates anterograde melanosome transport by recruiting kinesin-1 to melanosomes through interaction with SKIP. *Sci. Rep.* **5**, 8238. doi:10.1038/srep08238

Jiang, M., Esteve-Rudd, J., Lopes, V. S., Diemer, T., Lillo, C., Rump, A. and Williams, D. S. (2015). Microtubule motors transport phagosomes in the RPE, and lack of KLC1 leads to AMD-like pathogenesis. *J. Cell Biol.* **210**, 595-611. doi:10.1083/jcb.201410112

Johnson, H. W. and Schell, M. J. (2009). Neuronal IP3 3-kinase is an F-actin-bundling protein: role in dendritic targeting and regulation of spine morphology. *Mol. Biol. Cell* **20**, 5166-5180. doi:10.1091/mbc.e09-01-0083

Klomp, A. E., Teofilo, K., Legacki, E. and Williams, D. S. (2007). Analysis of the linkage of MYRIP and MYO7A to melanosomes by RAB27A in retinal pigment epithelial cells. *Cell Motil. Cytoskeleton* **64**, 474-487. doi:10.1002/cm.20198

Kulkarni, A., Khan, Y. and Ray, K. (2017). Heterotrimeric kinesin-2, together with kinesin-1, steers vesicular acetylcholinesterase movements toward the synapse. *FASEB J.* **31**, 965-974. doi:10.1096/fj.201600759RRR

Kuroda, T. S. and Fukuda, M. (2005). Functional analysis of Slac2-c/MyRIP as a linker protein between melanosomes and myosin VIIa. *J. Biol. Chem.* **280**, 28015-28022. doi:10.1074/jbc.M501465200

LaVail, M. M. (1976). Rod outer segment disk shedding in rat retina: relationship to cyclic lighting. *Science* **194**, 1071-1074. doi:10.1126/science.982063

Lim, A., Rechtsteiner, A. and Saxton, W. M. (2017). Two kinesins drive anterograde neuropeptide transport. *Mol. Biol. Cell* **28**, 3542-3553. doi:10.1091/mbc.e16-12-0820

Liu, X., Ondek, B. and Williams, D. S. (1998). Mutant myosin VIIa causes defective melanosome distribution in the RPE of shaker-1 mice. *Nat. Genet.* **19**, 117-118. doi:10.1038/470

Liu, X., Udovichenko, I. P., Brown, S. D. M., Steel, K. P. and Williams, D. S. (1999). Myosin VIIa participates in opsin transport through the photoreceptor cilium. *J. Neurosci.* **19**, 6267-6274. doi:10.1523/JNEUROSCI.19-15-06267.1999

Lopes, V. S., Ramalho, J. S., Owen, D. M., Karl, M. O., Strauss, O., Futter, C. E. and Seabra, M. C. (2007a). The ternary Rab27a-Myrip-Myosin VIIa complex regulates melanosome motility in the retinal pigment epithelium. *Traffic* **8**, 486-499. doi:10.1111/j.1600-0854.2007.00548.x

Lopes, V. S., Wasmeier, C., Seabra, M. C. and Futter, C. E. (2007b). Melanosome maturation defect in Rab38-deficient retinal pigment epithelium results in instability of immature melanosomes during transient melanogenesis. *Mol. Biol. Cell* **18**, 3914-3927. doi:10.1091/mbc.e07-03-0268

Marks, M. S. and Seabra, M. C. (2001). The melanosome: membrane dynamics in black and white. *Nat. Rev. Mol. Cell Biol.* **2**, 738-748. doi:10.1038/35096009

Moreiras, H., Lopes-da-Silva, M., Seabra, M. C. and Barral, D. C. (2019). Melanin processing by keratinocytes: A non-microbial type of host-pathogen interaction? *Traffic* **20**, 301-304. doi:10.1111/tra.12638

Narendra, A., Greiner, B., Ribi, W. A. and Zeil, J. (2016). Light and dark adaptation mechanisms in the compound eyes of Myrmecia ants that occupy discrete temporal niches. *J. Exp. Biol.* **219**, 2435-2442. doi:10.1242/jeb.142018

Pfeifer, A., Brandon, E. P., Kootstra, N., Gage, F. H. and Verma, I. M. (2001). Delivery of the Cre recombinase by a self-deleting lentiviral vector: efficient gene targeting in vivo. *Proc. Natl. Acad. Sci. USA* **98**, 11450-11455. doi:10.1073/pnas.201415498

Provance, D. W., Jr., Wei, M., Ipe, V. and Mercer, J. A. (1996). Cultured melanocytes from dilute mutant mice exhibit dendritic morphology and altered melanosome distribution. *Proc. Natl. Acad. Sci. USA* **93**, 14554-14558. doi:10.1073/pnas.93.25.14554

Raposo, G. and Marks, M. S. (2007). Melanosomes–dark organelles enlighten endosomal membrane transport. *Nat. Rev. Mol. Cell Biol.* **8**, 786-797. doi:10.1038/nrm2258

Robinson, C. L., Evans, R. D., Briggs, D. A., Ramalho, J. S. and Hume, A. N. (2017). Inefficient recruitment of kinesin-1 to melanosomes precludes it from facilitating their transport. *J. Cell Sci.* **130**, 2056-2065. doi:10.1242/jcs.186064

Schraermeyer, U., Peters, S., Thumann, G., Kociok, N. and Heimann, K. (1999). Melanin granules of retinal pigment epithelium are connected with the lysosomal degradation pathway. *Exp. Eye Res.* **68**, 237-245. doi:10.1006/exer.1998.0596

Tuma, M. C., Zill, A., Le Bot, N., Vernos, I. and Gelfand, V. (1998). Heterotrimeric kinesin II is the microtubule motor protein responsible for pigment dispersion in Xenopus melanophores. *J. Cell Biol.* **143**, 1547-1558. doi:10.1083/jcb.143.6.1547

Udovichenko, I. P., Gibbs, D. and Williams, D. S. (2002). Actin-based motor properties of native myosin VIIa. *J. Cell Sci.* **115**, 445-450.

Vancoillie, G., Lambert, J., Mulder, A., Koerten, H. K., Mommaas, A. M., Van Oostveldt, P. and Naeyaert, J. M. (2000). Kinesin and kinectin can associate with the melanosomal surface and form a link with microtubules in normal human melanocytes. *J. Invest. Dermatol.* **114**, 421-429. doi:10.1038/jid.2000.3

Volland, S., Esteve-Rudd, J., Hoo, J., Yee, C. and Williams, D. S. (2015). A comparison of some organizational characteristics of the mouse central retina and the human macula. *PLoS ONE* **10**, e0125631. doi:10.1371/journal.pone.0125631

Wasmeier, C., Hume, A. N., Bolasco, G. and Seabra, M. C. (2008). Melanosomes at a glance. *J. Cell Sci.* **121**, 3995-3999. doi:10.1242/jcs.040667

Wei, Q., Wu, X. and Hammer, J. A.III (1997). The predominant defect in dilute melanocytes is in melanosome distribution and not cell shape, supporting a role for myosin V in melanosome transport. *J. Muscle Res. Cell Motil.* **18**, 517-527. doi:10.1023/A:1018659117569

Weil, D., Blanchard, S., Kaplan, J., Guilford, P., Gibson, F., Walsh, J., Mburu, P., Varela, A., Levilliers, J., Weston, M. D. et al. (1995). Defective myosin VIIA gene responsible for Usher syndrome type 1B. *Nature* **374**, 60-61. doi:10.1038/374060a0

Williams, D. S. (1982). Ommatidial structure in relation to turnover of photoreceptor membrane in the locust. *Cell Tissue Res.* **225**, 595-617. doi:10.1007/BF00214807

Williams, D. S. and Lopes, V. S. (2011). The many different cellular functions of MYO7A in the retina. *Biochem. Soc. Trans.* **39**, 1207-1210. doi:10.1042/BST0391207

Williams, M. A., Pinto, L. H. and Gherson, J. (1985). The retinal pigment epithelium of wild type (C57BL/6J +/+) and pearl mutant (C57BL/6J pe/pe) mice. *Invest. Ophthalmol. Vis. Sci.* **26**, 657-669.

Wu, X. and Hammer, J. A. (2014). Melanosome transfer: it is best to give and receive. *Curr. Opin. Cell Biol.* **29**, 1-7. doi:10.1016/j.ceb.2014.02.003

Wu, X., Bowers, B., Rao, K., Wei, Q. and Hammer, J. A.III (1998). Visualization of melanosome dynamics within wild-type and dilute melanocytes suggests a paradigm for myosin V function In vivo. *J. Cell Biol.* **143**, 1899-1918. doi:10.1083/jcb.143.7.1899

Xia, C., Rahman, A., Yang, Z. and Goldstein, L. S. (1998). Chromosomal localization reveals three kinesin heavy chain genes in mouse. *Genomics* **52**, 209-213. doi:10.1006/geno.1998.5427

Xia, C.-H., Roberts, E. A., Her, L.-S., Liu, X., Williams, D. S., Cleveland, D. W. and Goldstein, L. S. B. (2003). Abnormal neurofilament transport caused by targeted disruption of neuronal kinesin heavy chain KIF5A. *J. Cell Biol.* **161**, 55-66. doi:10.1083/jcb.200301026

Yi, J., Wu, X. S., Crites, T. and Hammer, J. A.III (2012). Actin retrograde flow and actomyosin II arc contraction drive receptor cluster dynamics at the immunological synapse in Jurkat T cells. *Mol. Biol. Cell* **23**, 834-852. doi:10.1091/mbc.e11-08-0731

Young, R. W. (1967). The renewal of photoreceptor cell outer segments. *J. Cell Biol.* **33**, 61-72. doi:10.1083/jcb.33.1.61

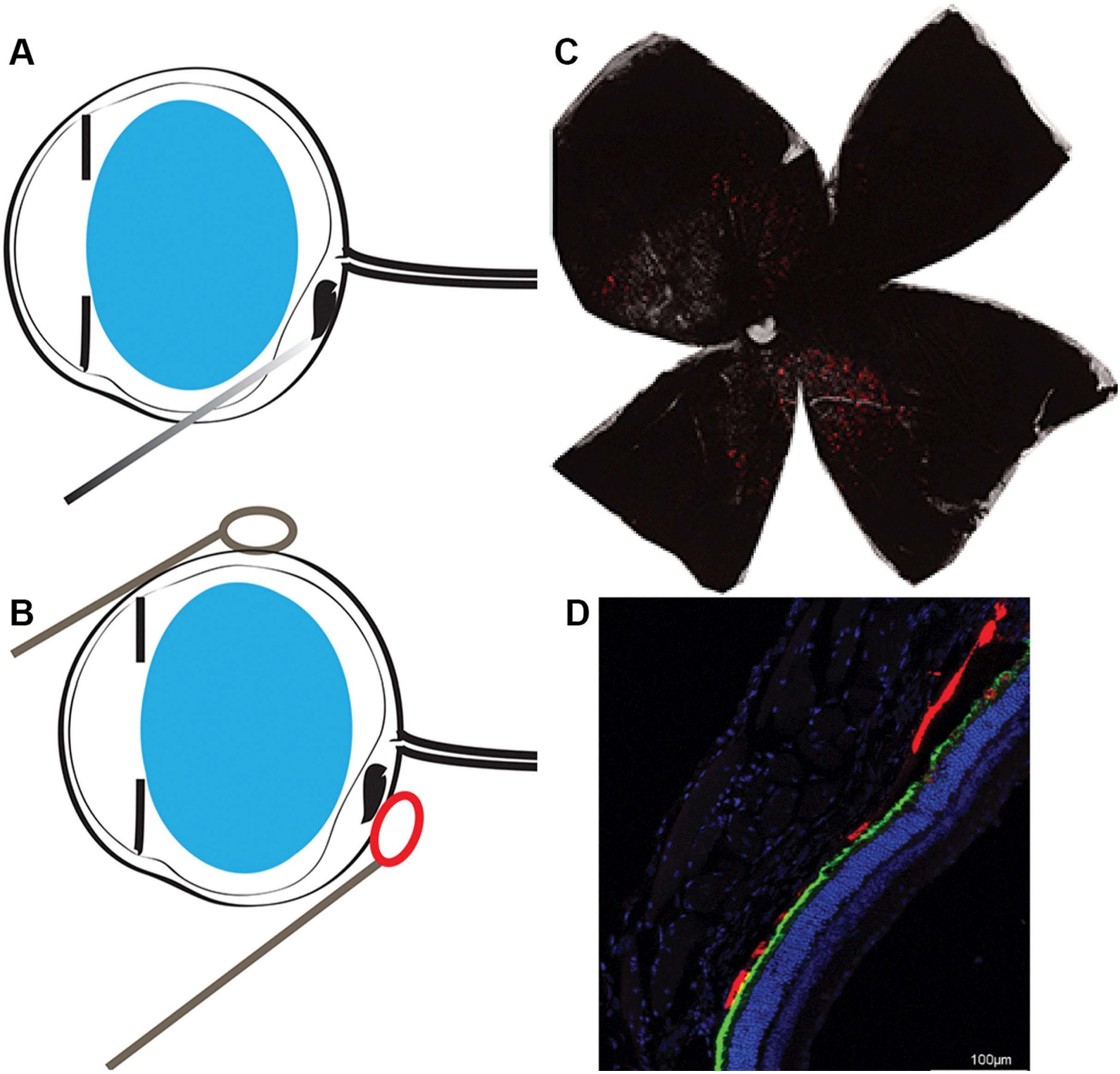

Figure S1.
Subretinal injection and electroporation of vectors expressing DYNC1H1 sh RNA or scrambled sh RNA. Schematic illustration of (A) subretinal injection, and, (B) electroporation. (C) Fluorescence microscope image of a retinal whole-mount. Red, DYNC1H1 shRNA-mCherry. (D) Representative cryosection, labeled with RHO antibodies to indicate photoreceptor outer segments (green), from an electroporated eye, injected with DYNC1H1shRNA-mCherry (red).

Journal of Cell Science • Supplementary information

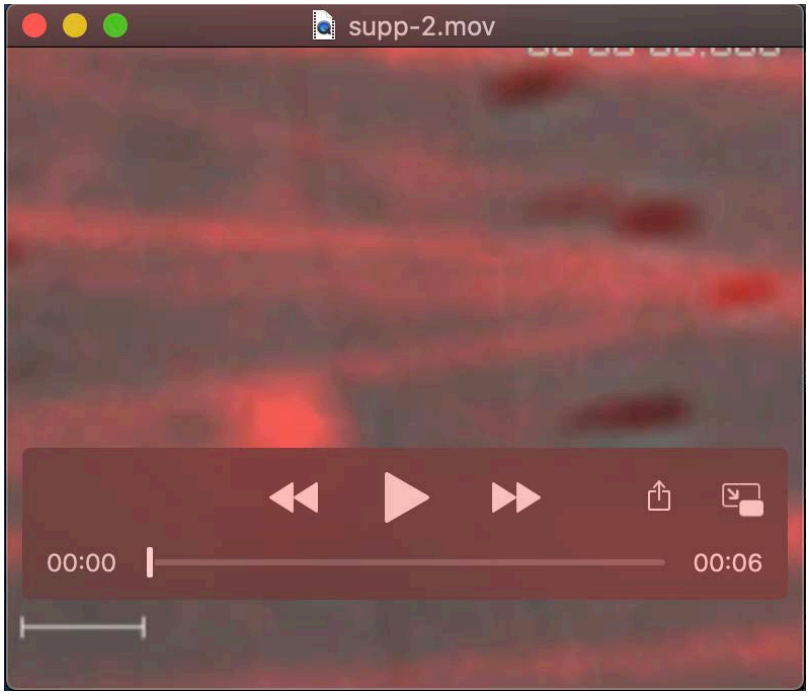

Movie 1. Movements of melanosomes along actin in an RPE cell. Cultured WT primary mouse RPE cells transduced with CellLight actin-RFP. Single z-plane images were collected by a spinning disk confocal microscope at 2 frames per second for 30 seconds. The playback rate of the movie is 10 frames per second (i.e. 5x real speed). Scale = 2 μm.

Journal of Cell Science • Supplementary information

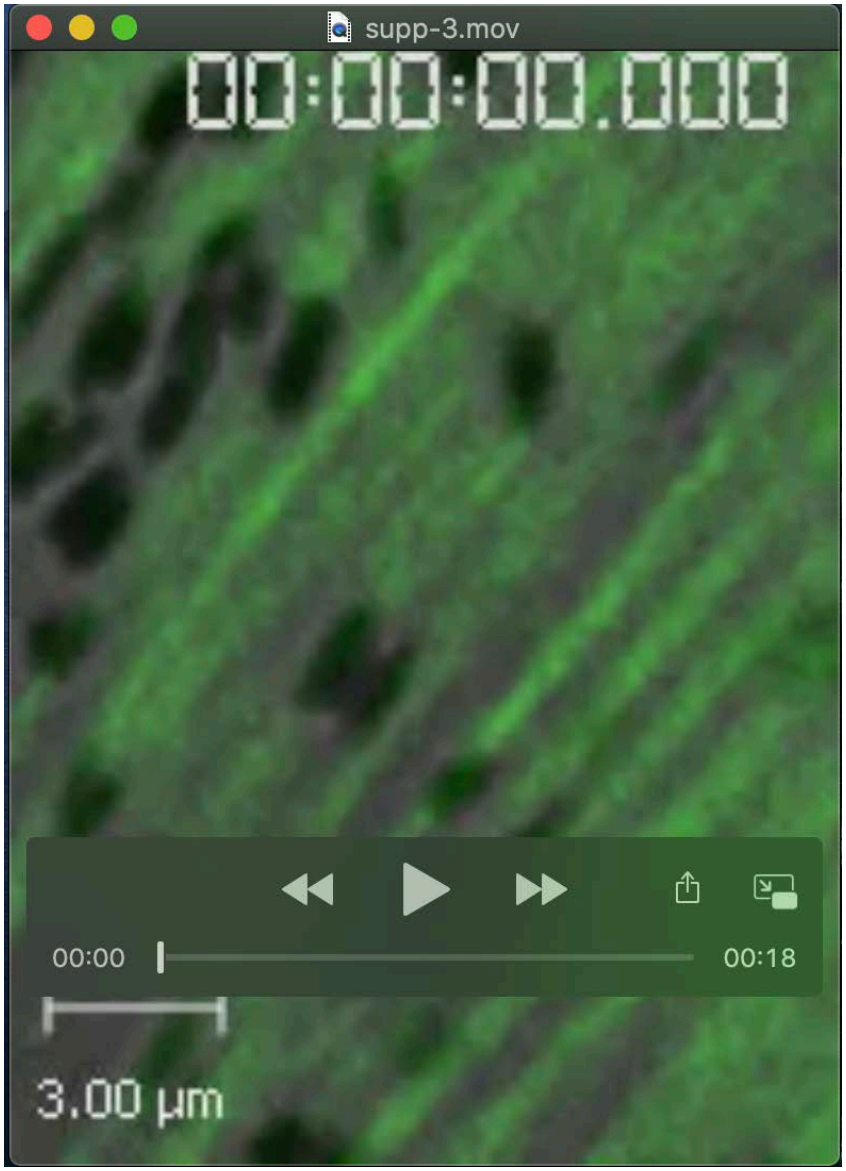

Movie 2. Movements of melanosomes along actin in an RPE cell. Cultured WT primary mouse RPE cells transfected with F-tractin-GFP. Single z-plane images were collected by a spinning disk confocal microscope at 2 frames per sec for 3 minutes. The playback rate of the movie is 20 frames per second (i.e. 10x real speed). Scale = 3 µm.

Journal of Cell Science • Supplementary information

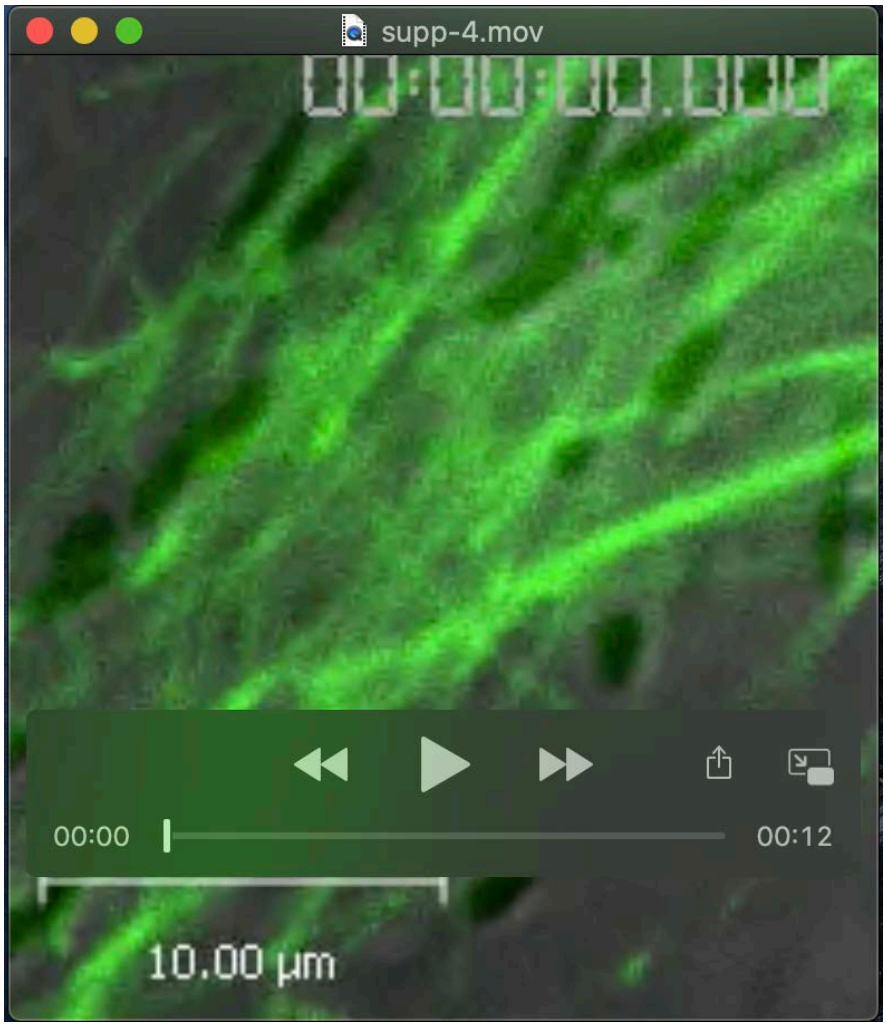

Movie 3. Movements of melanosomes along microtubules in an RPE cell. Cultured primary shaker1 mouse RPE cells (*Myo7a*-null) were transfected to express EB3-EGFP. While the EB3-EGFP labels most of each microtubule, it is concentrated more at the plus end. Single z-plane images were collected by a spinning disk confocal microscope at 2 frames per second for 1 minute. The playback rate of the movie is 10 frames per second (i.e. 5x real speed). Scale = 10 µm.

Journal of Cell Science • Supplementary information